Initial Steps of Aromatic Ring Formation in a Laminar Premixed Fuel-Rich Cyclopentene Flame†

N. Hansen,*,‡ T. Kasper,§ S. J. Klippenstein,|| P. R. Westmoreland,⊥ M. E. Law,⊥ C. A. Taatjes,‡ K. Kohse-Höinghaus,§ J. Wang,# and T. A. Cool#

Combustion Research Facility, Sandia National Laboratories, Livermore, California 94551, Department of Chemistry, Bielefeld University, D-33615 Bielefeld, Germany, Chemistry Division, Argonne National Laboratory, Argonne, Illinois 60439, Department of Chemical Engineering, University of Massachusetts, Amherst, Massachusetts 01003, and School of Applied and Engineering Physics, Cornell University, Ithaca, New York 14853

Received: December 4, 2006; In Final Form: January 11, 2007

A fuel-rich, nonsooting, premixed laminar cyclopentene flame ($\phi = 2.0$) at 37.6 Torr (50 mbar) is investigated by flame-sampling photoionization molecular-beam mass spectrometry utilizing vacuum-ultraviolet synchrotron radiation. Mole fractions as a function of distance from the burner are measured for 49 intermediates with ion masses ranging from 2 (H_2) to 106 (C_8H_{10}), providing a broad database for flame modeling studies. The isomeric composition is resolved for most species, and the identification of several C_4H_x, C_7H_6, and C_7H_8 isomers is discussed in detail. The presence of $C_5H_5CCH/C_5H_4CCH_2$ and cycloheptatriene is revealed by comparisons between flame-sampled photoionization efficiency data and theoretical simulations, based on calculated ionization energies and Franck−Condon factors. This insight suggests a new potential molecular-weight growth mechanism that is characterized by C_5-C_7 ring enlargement reactions.

1. Introduction

The formation of polycyclic aromatic hydrocarbons (PAHs) and soot is one of the most challenging chemical issues in combustion science today. The interest in this subject stems mostly from the fact that serious environmental concerns and health risks are associated with pollutant emissions from combustion devices.[1−4] Present understanding of the complex chemistry involved in PAH and soot formation is still incomplete. However, for any pollution control strategy involving prediction of the products of molecular-weight growth, a fundamental, molecular-level understanding of PAH and soot formation and of the associated combustion chemistry is crucial.

A prominent focus in combustion chemistry research is the production of the "first aromatic ring" species, including benzene and naphthalene, as this may be the rate-limiting step in the formation of larger PAHs and soot.[5−7] Earlier studies have revealed that the recombination of propargyl radicals (C_3H_3) appears to provide the dominant pathway to benzene (or phenyl + H) in most flames.[5,7,8] However, a number of other pathways may also be of importance, depending on the chemical structure of the fuel.[6,9−12] A recent review paper by McEnally et al. discusses the underlying chemistry and provides numerous references.[13] Several potential reaction sequences forming two-ring aromatic hydrocarbons such as indene and naphthalene and/or their respective indenyl and naphthyl radicals from nonaromatic precursors have been discussed in the literature.[14−17] In general, it is believed that resonantly stabilized radicals often accumulate to high concentrations and play a crucial role in aromatics formation.

Comparison of experimental data to models employing detailed chemical kinetics is essential for determining important chemical pathways in combustion and for understanding pollutant formation in combustion systems.[18,19] Due to the lack of knowledge about their detailed chemistry, most C_5 combustion intermediates are absent from current flame chemistry models. A notable exception is the resonance-stabilized cyclo-C_5H_5 (cyclopentadienyl) radical. Several specific routes have been proposed for converting cyclopentadienyl to aromatic species.[14−17,20,21] The radical−radical reaction of cyclo-C_5H_5 with CH_3 is supposed to be partially responsible for benzene formation, the reaction of cyclo-C_5H_5 with acetylene is a potential source for benzyl radicals in many fuel-rich flames, and the cyclo-C_5H_5 self-recombination is a possible pathway to naphthalene. As a consequence, cyclopentadienyl is believed to be an important intermediate supporting the growth of higher hydrocarbons, PAH, and soot in rich flames. The importance of other C_5 species in the growth of higher hydrocarbons in combustion is at this point rather unclear. Nevertheless, Pope and Miller suggested that *i*-C_5H_3 could react with CH_3 to form benzene, fulvene, or phenyl + H.[21]

This paper is part of our ongoing study of combustion chemistry and molecular weight growth by flame-sampling molecular beam photoionization mass spectrometry employing vacuum-ultraviolet (vacuum-UV) synchrotron radiation.[22] In some of our previous work, the combustion chemistry of rich flames fueled by propane, allene, and propyne was described.[23,24] Furthermore, several nonsooting fuel-rich flames, including fuel-rich allene, propyne, and cyclopentene flames, were used to identify C_3H_2, C_4H_3, C_4H_5, and C_5H_x ($x = 3-8$) isomers.[25−27]

† Part of the special issue "James A. Miller Festschrift".

* Corresponding author. Phone: (925) 294-6272. Fax: (925) 294-2276. E-mail: nhansen@sandia.gov.

‡ Sandia National Laboratories.

§ Bielefeld University.

|| Argonne National Laboratory.

⊥ University of Massachusetts.

Cornell University.

10.1021/jp0683317 CCC: $37.00 © 2007 American Chemical Society
Published on Web 02/15/2007

In view of the potential importance of C_5 species, the present study is concerned with cyclopentene combustion chemistry under fuel-rich conditions. The fuel cyclopentene is attractive for studies because the abstraction of hydrogen atoms forms several key flame intermediates in high concentrations, including the cyclopentadienyl and cyclopentenyl radicals. Thus, in this flame the importance of C_5 intermediates is enhanced compared to C_3 species. Furthermore, studying a fuel-rich cyclopentene flame is of particular interest as it closes the gap between small hydrocarbons and the larger, more complex hydrocarbons that constitute all liquid combustion fuels.

Nevertheless, investigations of the combustion chemistry of cyclopentene are scarce. McEnally and Pfefferle used non-premixed methane/air flames doped with cyclopentene to study hydrocarbon growth processes.[28] Lamprecht et al.[29] employed electron ionization (EI) mass spectrometry to study cyclopentene flames with different stoichiometries. Modeling efforts were undertaken later by Lindstedt and Rizos[14] and recently by Kamphus et al.[30]

This study is concerned with the initial steps of aromatic ring formation in a laminar premixed cyclopentene flame:

(a) To assist in flame chemistry modeling, experimental mole fraction profiles of 49 species with masses ranging from 2 (H_2) to 106 (C_8H_{10}) are determined. The thorough analysis of the flame data provides profiles of single-ring aromatic species and their C_3, C_4, and C_5 precursors. This study complements the existing database for a particular cyclopentene flame[29] with isomer specific information. The isomeric compositions are resolved for most intermediates; for example, the isomers of C_4H_4, C_4H_6, and C_4H_8 are identified.

(b) The presence of $C_5H_5CCH/C_5H_4CCH_2$ and cycloheptatriene is confirmed by comparison of photoionization efficiency measurements with simulations based on calculated ionization energies and Franck−Condon factors. The existence of $C_5H_5CCH/C_5H_4CCH_2$ and cycloheptatriene points toward C_5-C_7 ring enlargement reactions[31] as potential new pathways in molecular-weight growth mechanisms.

2. Experiment

The experiment is carried out in the low-pressure premixed flame apparatus at the Chemical Dynamics Beamline at the Advanced Light Source (ALS) at the Lawrence Berkeley National Laboratory. The technique of flame-sampling molecular-beam photoionization time-of-flight (TOF) mass spectrometry is fully described elsewhere.[22]

In the present experiment, the investigated flame is a cyclopentene/oxygen/25% argon flame with a fuel/oxygen equivalence ratio $\phi = 2.0$ at a pressure of 37.6 Torr (50 mbar) and a cold-flow reagent velocity of 54.7 cm/s. The flame is shielded by an Ar shroud gas, and cyclopentene from Sigma-Aldrich (96%) is used without further purification.

Flame gases are sampled through the ~0.2 mm orifice of a quartz sampling cone on the flow axis of a flat-flame burner. Translation of the burner toward or away from the quartz sampling cone allows mass spectra to be taken at any desired position within the flame. A skimmer of 2.0 mm aperture placed 23 mm downstream on the axis of the expanded (10^{-4} Torr) jet forms a molecular beam that passes into the differentially pumped (10^{-6} Torr) ionization region, where it is crossed by tunable vacuum-ultraviolet light. The resulting photoions are separated by using pulsed-extraction time-of-flight mass spectrometry and detected with a multichannel plate. A multiscaler records the TOF mass spectra.

The ALS delivers tunable undulator radiation which is energy-selected by a 3 m off-plane Eagle monochromator. A rare-gas filter removes contributions from higher undulator harmonics, and an energy resolution of either 25 or 40 meV fwhm (full width at half-maximum, measured from the observed width of autoionizing resonances in O_2)[32,33] is employed. The photon current passing through the ionization region is measured with a silicon photodiode calibrated at the National Institute of Standards and Technology (NIST) for quantum efficiency (electron/photon) in the energy range from 8 to 17 eV.

To determine burner profiles and photoionization efficiencies (PIE), ion signals at a given m/z ratio are obtained by integration of the accumulated ion counts per channel over a 60 ns time interval centered about the mass peak, from which the baseline contribution, obtained from the signal between peaks, is subtracted. This approach permits integration over the entire temporal profile of each mass peak, while avoiding overlapping contributions from adjacent mass peaks. The baseline-corrected ion signals are corrected for the contributions of ^{13}C, ^{2}H, and ^{18}O isotopomers and finally are normalized by the photon current.

3. Species Identification

The power of the ALS flame experiment lies in the ability to easily tune the energy of the ionizing photons. This allows us to obtain data which show the signal taken at a particular position in the flame as a function of mass and photon energy. The so-called photoionization efficiency (PIE) spectrum for a given mass is a valuable tool for determining the isomeric composition of combustion intermediates.[22,25−27,34−36] Isomeric species have in general very different chemical behaviors, and therefore, experimental determinations of isomeric compositions are critically needed.

In this paper we show how different C_4H_4, C_4H_6, and C_4H_8 isomers are identified by comparing flame-sampled photoionization efficiency curves with cold-flow PIE spectra of the pure substances. This work and that reported previously[26,27] provide successful identification of most C_4H_x and C_5H_x isomers in the fuel-rich cyclopentene flame.

We also identify various C_7H_6 and C_7H_8 isomers by comparing the experimental PIE spectra with theoretical simulations based on calculated ionization energies and Franck−Condon factors. Theoretical simulations analogous to those reported in ref 27 are employed. In particular, rovibrational properties are obtained from B3LYP/6-311++G**[37,38] density functional calculations using the Gaussian 98 software[39] and unrestricted spin wavefunctions. Theoretical ionization energies and heats of formation are obtained from an approximation to QCISD(T)/6-311++G(3df,2pd) energies given by E[QCISD(T)/6-311G**] + E[MP2/6-311++G(3df,2pd)] − E[MP2/6-311G**], with these energies being obtained with the MOLPRO quantum chemistry package[40] and employing spin-restricted wavefunctions. The heats of formation determinations employ CH_4 and H_2 as reference species.

3.1. Identification of C_4H_4, C_4H_6, and C_4H_8 (C_3H_4O) Isomers. Figure 1 summarizes the identification of different C_4H_4, C_4H_6, and C_4H_8 (or C_3H_4O) isomers. Flame-sampled photoionization efficiency curves are compared with photoionization efficiencies measured in a cold-flow of the pure substance in Ar. Panel a shows the flame-sampled photoionization efficiency data for $m/z = 52$ and the cold-flow PIE spectrum of CH_2CHCCH (vinylacetylene). The near-equivalence of the two datasets is remarkable. Vinylacetylene is easily identified by broad autoionization features at 9.63, 9.88, and

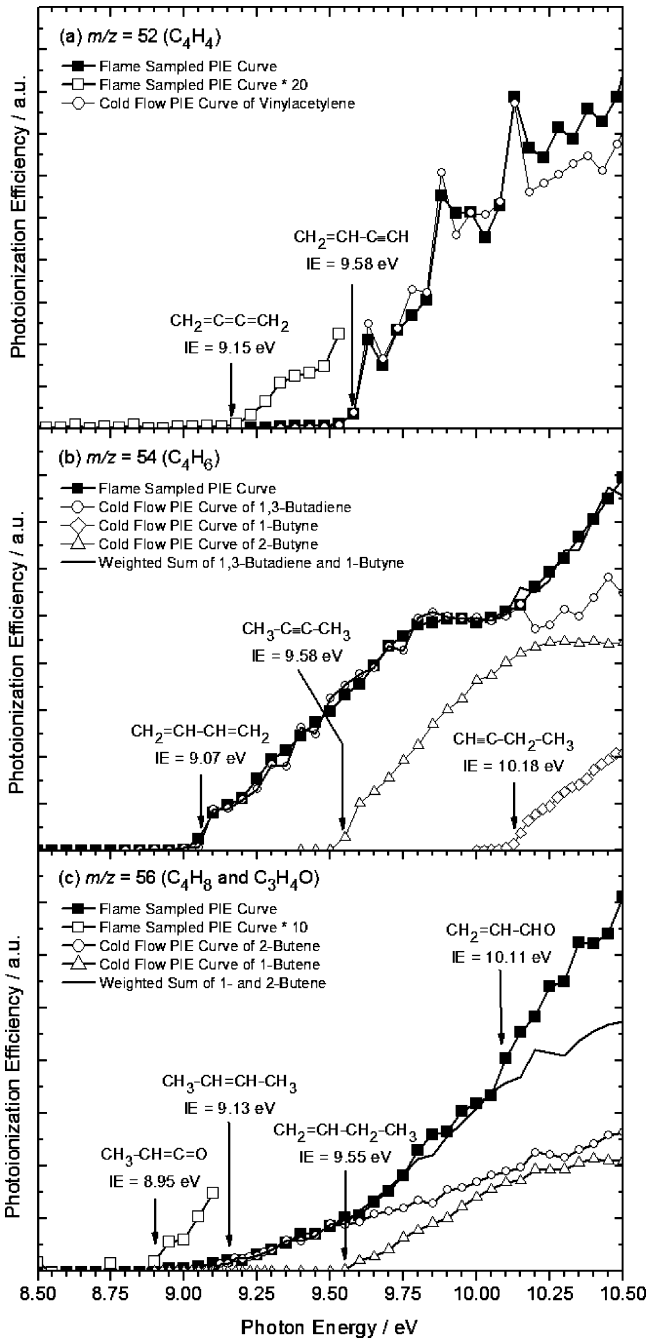

Figure 1. (a) Comparison of the flame-sampled PIE curve for $m/z = 52$ and the PIE spectrum of vinylacetylene. Species at $m/z = 52$ are identified as 1,2,3-butatriene and vinylacetylene. (b) Comparison of the flame-sampled PIE curve for $m/z = 54$ and the PIE spectra of 1,3-butadiene and 1- and 2-butynes. The presence of 1,3-butadiene and 1-butyne is confirmed, while 2-butyne seems to be absent. (c) Comparison of the flame-sampled PIE curve for $m/z = 56$ with PIE spectra for 1- and 2-butenes. The presence of 1- and 2-butenes is revealed; signal below 9.1 and above 10.1 eV might be attributed to the presence of CH_3CHCO and CH_2CHCHO isomers.

10.13 eV in the PIE spectrum.[41] The signal below the ionization energy (IE = 9.58 eV) of vinylacetylene[42] is attributed to CH_2CCCH_2 (1,2,3-butatriene), which is identified by its ionization energy.[43]

In Figure 1b the flame-sampled photoionization efficiency spectrum for $m/z = 54$ is compared with photoionization efficiencies measured for $CH_2CHCHCH_2$ (1,3-butadiene), $CHCCH_2CH_3$, and CH_3CCCH_3 (1- and 2-butyne). A weighted sum of the 1,3-butadiene and the 1-butyne photoionization efficiencies can explain the flame-sampled spectra. 2-Butyne appears to be absent from this cyclopentene flame, as does 1,2-butadiene which has an ionization energy of 9.23 eV.[44]

Identification of the species present at $m/z = 56$ is harder to accomplish. We clearly identify $CH_2CHCH_2CH_3$ and CH_3-$CHCHCH_3$ (1- and 2-butene) by comparing the flame-sampled photoionization efficiency curve with cold-flow photoionization spectra of those two isomers as shown in Figure 1c. Possible contributions from $CH_3C(CH_3)CH_2$ (isobutene), which has an ionization energy of 9.22 eV,[45] cannot be ruled out completely since the corresponding cold-flow PIE spectrum has not been measured. Nevertheless, the good agreement between 9.1 and 9.5 eV of the flame-sampled data and the cold-flow data of 2-butene suggests that a conceivable contribution of isobutene would be negligible. Signal below 9.13 eV, the ionization energy of 2-butene,[46] is attributed to the presence of methylketene, as identified by the observed ionization threshold of 8.95 eV.[47] The additional signal above 10.11 eV is probably due to the presence of 2-propenal, an isomeric form of methylketene.[48]

3.2. Identification of C_7H_6 Isomers. The photoionization efficiency curve for $m/z = 90$ in this cyclopentene flame is shown in Figure 2a. The spectrum is recorded at ~4 mm distance above the burner where the mole fraction profile of C_7H_6 peaks. A threshold near 8.2 eV can be clearly seen. The identification of C_7H_6 isomers is based on a comparison between the flame-sampled PIE curve and theoretical simulations based on calculated ionization energies and Franck−Condon factors. Ionization energies and heats of formation of several isomers of C_7H_6 are calculated and summarized in Table 1. We exclude any linear and branched structures to reduce the considerable computational effort because it seems unlikely that the dominant C_7H_6 species are linear. Mole fraction profiles of typical linear flame species such as C_6H_2 and C_8H_2 are expected to peak after the fuel is consumed completely, and thus, they reach their maximum mole fractions at greater distances from the burner surface than the C_7H_6 species. The present burner profile for C_7H_6 (see below) shows an overlap with those for potential cyclic C_5 and C_6 precursor molecules. For this reason, ring structures seem to be more likely candidates to be present at this particular position in the cyclopentene flame.

The five-membered ring molecule $C_5H_4CCH_2$ is the most stable isomer with a calculated heat of formation (0 K) of 86.8 kcal/mol. Just slightly higher in energy are the three isomers of C_5H_5CCH. Their heats of formation range from 89.2 to 96.3 kcal/mol (see Table 1). The bicyclic species $-C_6H_4-CH_2-$ and $-C_5H_4-CHCH-$ are also included in Table 1 as possible C_7H_6 isomers. The calculated heat of formation of bicyclic $-C_6H_4-CH_2-$ (93.2 kcal/mol) is comparable to those for the C_5H_5CCH isomers. Meanwhile, the bicyclic $-C_5H_4-CHCH-$ is less stable than the bicyclic $-C_6H_4-CH_2-$ by about 15 kcal/mol. A comparable heat of formation of 98.4 kcal/mol is calculated for the seven-membered ring structure cyclo-C_7H_6 (-CHCHCH-CHCHCHC-). Possible three- and four-membered ring structures are not considered since they are not likely to be present at high concentrations at the elevated flame temperatures.

We further consider possible contributions from radical species. The six-membered ring structures of the C_6H_5-CH and $C_6H_4-CH_2$ type radicals are higher in energy than the five-membered ring molecules: The heats of formation of the triplet ground states are calculated to be ~112 kcal/mol, and according to our calculations, the singlet−triplet splittings for those radicals are about 5−25 kcal/mol.

The presence of the bicyclic species, the six-membered ring radicals, and the cyclo-C_7H_6 species in the cyclopentene flame

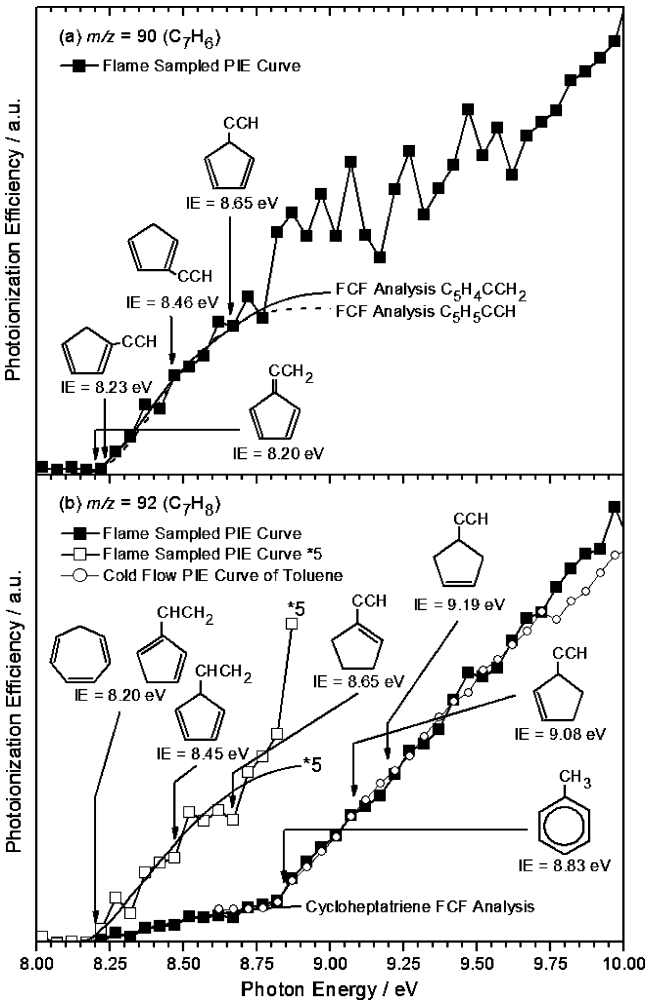

Figure 2. Comparison between flame-sampled PIE curve for (a) $m/z = 90$ (C_7H_6) and (b) $m/z = 92$ (C_7H_8) with the PIE spectra simulated on the basis of a Franck−Condon factor analysis and the cold-flow PIE spectrum of toluene. Calculated ionization energies of some isomers are indicated. (a) The cyclic species -CHCHCHCHC(C═CH_2)- or -CH_2CHCHCHCH(C≡CH)- are identified by their ionization thresholds and the Franck−Condon factor analysis. Contributions from -CHCHCH_2-CHC(C≡CH)- and -CHCHCHCHCH(C≡CH)- can be ruled out. (b) The Franck−Condon factor analysis reveals that the experimental PIE curve between 8.2 and 8.8 eV can be explained by the presence of the cycloheptatriene. Signal above 8.8 eV is dominated by toluene. The PIE spectrum of toluene is shifted vertically to compensate for contributions from other isomers near 8.8 eV.

can be excluded by comparing the calculated ionization energies with the observed threshold in the PIE spectra (Figure 2a). The calculated adiabatic ionization energy of 8.75 eV for bicyclic-C_6H_4−CH_2- is well above the observed threshold near 8.2 eV, while the calculated adiabatic ionization energies of the C_6H_5-CH, C_6H_4−CH_2, and cyclo-C_7H_6 isomers are well below the observed threshold. Furthermore, those radical species and bicyclic-C_5H_4−CHCH- are less stable by about ∼20 kcal/mol compared to the most stable -CHCHCHCHC(C═CH_2)- isomer and are therefore probably not abundant in high concentrations.

The calculated ionization energies of 8.20 eV for -CHCHCHCHC(C═CH_2)- and 8.23 eV for -CH_2CHCHCHC-(C≡CH)- agree within the experimental and computational error limits with the observed threshold near 8.2 eV. In a photoelectron spectroscopy study, Müller et al. determined a slightly higher ionization threshold for -CHCHCHCHC(C═CH_2)- of 8.29 eV.[49] The -CHCHCH_2CHC(C≡CH)- and -CHCHCHCHCH-(C≡CH)- isomers may contribute to the observed PIE curve above their ionization energies of 8.46 and 8.65 eV, respectively.

TABLE 1: Ionization Energies and Heats of Formation of Five- and Six-Membered Ring C_7H_6 Isomers

species	ionization energy (eV) calc	lit.	$\Delta_f H^0$(0K) (kcal/mol)	ref
-CHCHCHCHC(C═CH_2)-	8.20	8.29, 8.88	86.8	49,72
-CH_2CHCHCHC(C≡CH)-	8.23		89.2	
-CHCHCH_2CHC(C≡CH)-	8.46		90.2	
-CHCHCHCHCH(C≡CH)-	8.65		96.3	
cyclo-C_7H_6 (-CHCHCHCHCHCHC-)	7.53		98.4	
bicyclic-C_6H_4-CH_2-	8.75	8.82	93.2	73,74
bicyclic-C_5H_4-CHCH-	8.49	8.41	108.9	49
^{3}-C_6H_5(CH)-	7.41		111.9	
^{1}-C_6H_5(CH)-	7.22		116.3	
^{3}-CCHCHCHCHC(CH_2)-	7.41		112.4	
^{1}-CCHCHCHCHC(CH_2)-	7.01		121.6	
^{3}-CHCHCCHCHC(CH_2)-	7.34		112.4	
^{1}-CHCHCCHCHC(CH_2)-	6.91		122.4	
^{3}-CHCCHCHCHC(CH_2)-	7.37		114.0	
^{1}-CHCCHCHCHC(CH_2)-	6.22		140.3	

To determine the isomeric composition of the C_7H_6 species, the photoionization efficiency spectrum is simulated on the basis of a Franck−Condon factor analysis analogous to the ones described earlier.[25−27,50] The calculations are carried out using a program developed by Winter et al.[51,52] The resulting Franck−Condon factors, including hot bands arising from thermal population at the assumed temperature of 300 K, are integrated and convolved with a Gaussian response function corresponding to the measured experimental photon energy resolution of 40 meV (fwhm). The results are also shown in Figure 2a.

The Franck−Condon factor analysis reveals that the -CHCHCHCHC(C═CH_2)- and the -CH_2CHCHCHC(C≡CH)- forms are hard to distinguish. The calculated near-threshold photoionization efficiency curves for both species look similar and fit the observed data between 8.2 and 8.7 eV quite well. An ionization energy of 8.23 ± 0.05 eV was determined for either the -CHCHCHCHC(C═CH_2)- or possibly the -CH_2-CHCHCHC(C≡CH)- isomer. However, the calculations suggest that we can rule out the presence of the -CHCHCH_2CHC(C≡CH)- and -CHCHCHCHCH(C≡CH)- isomers.

From the chemical point of view, the C_7H_6 isomers in the environment of the fuel-rich cyclopentene flame are likely formed by the C_5H_5 (cyclopentadienyl) + C_2H_2 (acetylene) ⇄ C_7H_6 + H reaction. This reaction has been studied theoretically by Fascella et al.,[31] who showed that the initial radical C_5H_5−CH═CH adduct can lose a hydrogen atom in an endothermic reaction to form the stable -CHCHCHCHCH(C≡CH)- product. However, no experimental evidence exists for the presence of this specific C_7H_6 isomer in the fuel-rich cyclopentene flame. In a second pathway, the initial C_5H_5−CH═CH adduct can undergo an exothermic 1,3-hydrogen shift reaction to recover the stability of the parent C_5H_5 ring and to form the resonantly stabilized $C_5H_4CHCH_2$ radical, as shown in eq 1. It seems plausible that the $C_5H_4CCH_2$ isomer is subsequently formed by hydrogen loss or abstraction.

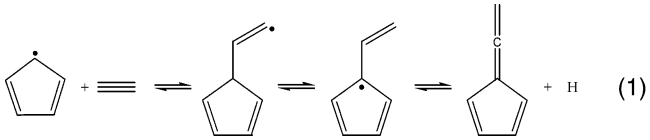

(1)

Possible pathways forming the -CH_2CHCHCHC(C≡CH)- isomer are less obvious. However, in the H-atom-rich environ-

TABLE 2: Ionization Energies and Heats of Formation of Cyclic C_7H_8 Isomers

species	ionization energy (eV) calc	ionization energy (eV) lit.	$\Delta_f H^0$(0K) (kcal/mol)	ref
$C_6H_5CH_3$ (toluene)	8.81	8.828	16.8	75
C_7H_8 (cycloheptatriene)	8.20	8.03, 8.29, 8.20	48.7	76, 77
-C(CH═CH_2)CH_2CHCHCH-	7.92		49.2	
-C(CH═CH_2)CHCH_2CHCH-	8.20		50.1	
-CH(CH═CH_2)CHCHCHCH-	8.45		55.7	
-C(C═CH_2)CHCHCH_2CH_2-	8.07		65.1	
-C(C═CH_2)CH_2CHCHCH_2-	8.69		68.1	
-C(C≡CH)CH_2CH_2CH_2CH-	8.65		67.1	
-CH_2CH(C≡CH)CH_2CHCH-	9.19		70.8	
-CH(C≡CH)CH_2CH_2CHCH-	9.08		71.4	

ment of a fuel-rich flame it is conceivable that hydrogen atom migration around the cyclopentadiene ring takes place and converts the initial -CHCHCHCHCH(C≡CH)- isomer into the most stable -CH_2CHCHCHC(C≡CH)- tautomeric species:

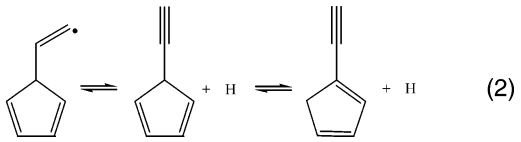

(2)

The C_7H_6 isomers are important intermediates in the formation of aromatic species in the fuel-rich cyclopentene flame. C_7H_6 might react with acetylene to ultimately form indene, or H-atom addition might open a new route to a five-membered ring C_7H_7 radical species which undergoes isomerization to form the resonantly stabilized cycloheptatrienyl or benzyl radicals:[31]

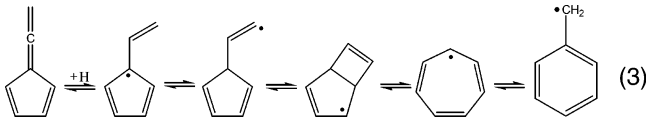

(3)

Both radical species, cycloheptatrienyl and benzyl, are quite stable and thus they are good precursor candidates for forming multiring structures, including indene and naphthalene.[15,16,31]

3.3. Identification of C_7H_8 Isomers. The photoionization efficiency curve for $m/z = 92$ is shown in Figure 2b. A threshold near 8.2 eV is obvious. As for C_7H_6, the identification of the C_7H_8 isomers is based on a comparison between the flame-sampled PIE curve and models based on calculated ionization energies and Franck−Condon factors. C_7H_6 is identified to be either the $C_5H_4CCH_2$ or one of the C_5H_5CCH isomers. Thus, similar C_7H_8 isomers of the C_5H_7CCH, $C_5H_6CCH_2$, or C_5H_5-$CHCH_2$ type are conceivable. The calculated ionization energies and heats of formation of several isomers of C_7H_8 are summarized in Table 2. For the same reasons mentioned above, we again exclude any linear and branched structures.

Toluene and cycloheptatriene are clearly the most stable isomers with calculated heats of formation (0 K) of 16.8 and 48.7 kcal/mol. Just slightly higher in energy than cycloheptatriene are the three isomers of $C_5H_5CHCH_2$. Heats of formation for -C(CH═CH_2)CH_2CHCHCH-, -C(CH═CH_2)CHCH_2CHCH-, and -CH(CH═CH_2)CHCHCHCH- are calculated to be 49.2, 50.1, and 55.7 kcal/mol, respectively. All other five-membered ring structures, including the $C_5H_6CCH_2$ and C_5H_7CCH species, are less stable. The calculated heats of formation range from 65.1 kcal/mol for -C(C═CH_2)CHCHCH_2CH_2- to 71.4 kcal/mol for -CH(C≡CH)CH_2CH_2CHCH.

The calculated ionization energies (Table 2) of -C(CH═CH_2)CH_2CHCHCH- (7.92 eV) and -C(C═CH_2)CHCHCH_2CH_2- (8.07 eV) are below the observed threshold in the photoionization efficiency spectra (Figure 2b); therefore the presence of those isomers can be ruled out immediately. Other isomers might be hard to detect; for example, the ionization energies of -CH_2-CH(C≡CH)CH_2CHCH- (9.19 eV) and -CH(C≡CH)CH_2CH_2-CHCH- (9.08 eV) are above the ionization threshold of toluene. The photoionization efficiency spectrum of toluene is shown in Figure 2b, which is shifted vertically to compensate for contributions from other isomers below 8.8 eV. The comparison between the flame-sampled PIE curve and the cold-flow PIE spectrum of toluene indicates that, above 8.8 eV, the signal is dominated by toluene. Thus, the possible presence of those two C_5H_7CCH isomers can largely be ruled out.

The observed threshold near 8.2 eV can be explained by either the -C(CH═CH_2)CHCH_2CHCH- or the cycloheptatriene isomers, as the observed and calculated ionization energies agree perfectly. A comparison between the observed photoionization efficiency curve and the calculated ionization energies of -CH-(CH═CH_2)CHCHCHCH- (8.45 eV) and -C(C≡CH)CH_2CH_2-CH_2CH- (8.65 eV) might suggest the presence of those two isomers (Figure 2b).

The Franck−Condon factor analysis reveals that the cycloheptatriene and the -C(CH═CH_2)CHCH_2CHCH- isomers are difficult to distinguish. The calculated near-threshold photoionization efficiency curves for both species look similar and fit the observed data between 8.2 and 8.8 eV satisfactorily. Figure 2b shows the comparison between a calculated PIE curve for cycloheptatriene with the experimental data, and good agreement is obvious. A similar fit can be achieved by considering the five-membered -C(CH═CH_2)CHCH_2CHCH- ring species. However, from the chemical point of view, it is puzzling why the -C(CH═CH_2)CHCH_2CHCH- isomer should be the only detectable five-membered C_7H_8 species. We therefore conclude that signal above the observed threshold of 8.22 eV is due to the presence of cycloheptatriene.

Possible formation pathways of toluene, including reactions of methyl radicals with either phenyl or benzene, and the reaction of the resonantly stabilized CH_3CCCH_2 (1-methylallenyl) radicals with H_2CCH (propargyl) radicals are known and have been discussed in the recent models:[30]

$$C_6H_5 + CH_3 \rightleftharpoons C_6H_5CH_3 \quad (4)$$

$$C_6H_6 + CH_3 \rightleftarrows C_6H_5CH_3 + H \quad (5)$$

$$C_3H_3 + C_4H_5 \rightleftarrows C_6H_5CH_3 \quad (6)$$

Information about the combustion chemistry of cycloheptatriene is scarce, and formation pathways of cycloheptatriene are less obvious. The reaction between benzene and methylene is a potential direct route leading to cycloheptatriene. It can also be formed by isomerization of C_7H_8 isomers, including toluene or five-membered ring species, similar to the reactions discussed in eq 3.[31] A bimolecular reaction between cycloheptatrienyl and atomic hydrogen would also result in the formation of cycloheptatriene. The reverse reaction is a potential destruction pathway of cycloheptatriene, as is the isomerization to the more stable toluene.

4. Flame Analysis and Experimental Mole Fraction Profiles

Besides the species identification, the goals of this study are to assist in kinetic modeling and to help identify the main decomposition pathways of cyclopentene and the main routes toward formation of small aromatic hydrocarbons. For these purposes, mole fraction profiles of 49 key intermediates are

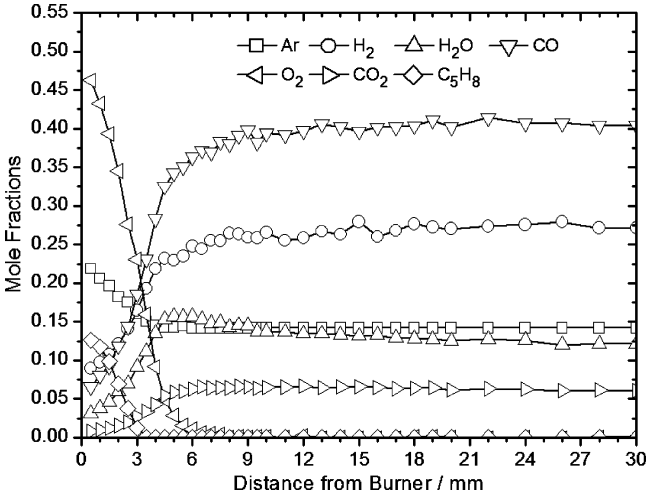

Figure 3. Experimental mole fraction profiles for the major species in the cyclopentene flame: H_2, H_2O, CO, O_2, Ar, CO_2, and C_5H_8.

determined and critically compared with previous experimental and modeling studies.[14,29,30]

In principle, it is possible to determine absolute mole fractions of every species, including different isomers, in each flame. A direct determination of the mole fractions requires knowledge of the respective cross-sections for photoionization of each species. For a large number of key combustion intermediates, absolute photoionization cross-sections have been measured.[41,53] Most of the available cross-sections have an uncertainty not greater than 15%. However, for some species, especially radicals, the photoionization cross-sections are hard to obtain experimentally. Nevertheless reasonable estimations for absolute photoionization cross-sections can be made on the basis of known cross-sections for molecules with similar functional groups. To this end, we consider the number of C=C double and C≡C triple bonds, the different ionization energies, and the photon energies used for the mole fraction determinations.[54]

The mole fractions are derived according to the method described by Cool et al.;[23] mass discrimination factors and photoionization cross-sections are taken from refs 41 and 53. Table 1 of the Supporting Information summarizes the critical parameters, i.e., mass discrimination factors, photon energies, and photoionization cross-sections, used for signal quantification. Species profiles are shifted by 0.5 mm to compensate for probe perturbation.

The accuracy of the mole fractions depends on a number of parameters, among them the quality of the cross-section and mass discrimination data, accumulation of background gases, and flame distortion introduced by the sampling probe. Therefore, the mole fractions for species with well-known cross-sections have a probable uncertainty of ±40%, while for species with unknown (estimated) photoionization cross-sections the mole fraction should be correct within a factor of 2−4. This level of accuracy is sufficient for many kinetic modeling purposes. When comparing mole fractions from different data sets, all error sources have to be taken into account.

4.1. Mole Fraction Profiles of Major Flame Species. Figure 3 shows the mole fraction profiles of the major flame species (H_2, H_2O, CO, O_2, Ar, CO_2, and C_5H_8) in the fuel-rich cyclopentene flame. H_2 and Ar profiles are measured at 16.20 eV, and H_2O, CO, O_2, and CO_2 profiles are measured at 14.35 eV, while the C_5H_8 profile is recorded at 9.40 eV. The following corrections and assumptions are applied: For the Ar profile, contributions from allene and propyne near the burner surface are neglected and the radial diffusion of Ar atoms from the shroud gas into the flame is corrected by assuming a constant Ar signal after it reaches its minimum near 5 mm distance from the burner. Contributions from C_2H_4 to the $m/z = 28$ signal are subtracted, while contributions from C_2H_4O isomers (acetaldehyde and ethenol) at $m/z = 44$ are neglected. The H_2O and O_2 ion signals are corrected for background contributions. We assume that 50% of the $m/z = 18$ ion signal at the burner surface and the remaining $m/z = 32$ signal in the exhaust gases originate from background.

Mole fraction profiles for H_2, CO, O_2, and CO_2 are also determined in a different way by applying target species to Ar signal ratios at every burner position at 16.20 eV. Calibration factors for the signal ratios of H_2, CO, O_2, and CO_2 to Ar are determined from cold gas flows in the range from 15.50 to 17.00 eV. In addition to the above-described corrections to the H_2O, CO, and O_2 signals, N_2 (IE = 15.58 eV),[55] background contributions at $m/z = 28$ need to be considered in this procedure. Mole fraction profiles derived in both ways agree perfectly.

The observed mole fraction profiles are compared against C, H, and O atom balances, and the maximum discrepancies of ∼2.5% for C and H and ∼1.0% for O are well within the precision of the photoionization measurements. A reasonable agreement of the major species profiles (H_2, H_2O, CO, Ar, CO_2, and C_5H_8) between the current photoionization mass spectrometric study and the earlier study by Lamprecht et al.[29] is observed. The newly derived profiles also show good agreement with earlier modeling results.[14,30]

According to Kamphus et al.,[30] cyclopentene consumption is dominated by elimination of H_2 to form cyclopentadiene:

$$\text{cyclo-}C_5H_8 \rightleftarrows \text{cyclo-}C_5H_6 + H_2 \qquad (7)$$

It is rather unusual for a thermal nonradical reaction to play an important role in fuel consumption, as radical additions and abstractions have much lower activation energies. Other significant channels for cyclopentene consumption are the reaction with H-atoms to form cyclopentenyl (cyclo-C_5H_7) radicals

$$\text{cyclo-}C_5H_8 + H \rightleftarrows \text{cyclo-}C_5H_7 + H_2 \qquad (8)$$

and the chemically activated H-atom addition/decomposition to make allyl and ethylene:[14]

$$\text{cyclo-}C_5H_8 + H \rightleftarrows C_3H_5 + C_2H_4 \qquad (9)$$

4.2. Mole Fraction Profiles for C_1 Species. The experimentally derived mole fraction profiles for CH_3 (methyl) and CH_4 (methane) are shown in Figure 4a. The CH_3 and CH_4 mole fractions peak at 1.6×10^{-3} near 3.5 mm from the burner and 4.5×10^{-3} near 3.0 mm, respectively, and both profiles show long tails going out all the way to 18 mm.

The present CH_3 and CH_4 mole fractions agree with the measurements from Lamprecht et al.[29] to within a factor of 2. However, the prior work determined CH_3 to be present in higher concentration than the CH_4, an inference which is not reproduced in the current experiment. Fragmentation distortions of signal intensities present major difficulties for the quantification of the earlier EI measurements. These distortions are especially problematic for low molecular weight radicals that are fragmentation products of a variety of flame species. Such distortions provide a likely explanation for the observed differences in CH_3 mole fractions.

4.3. Mole Fraction Profiles for C_2 Species. Figure 4b shows the experimentally derived mole fraction profiles for C_2H_2

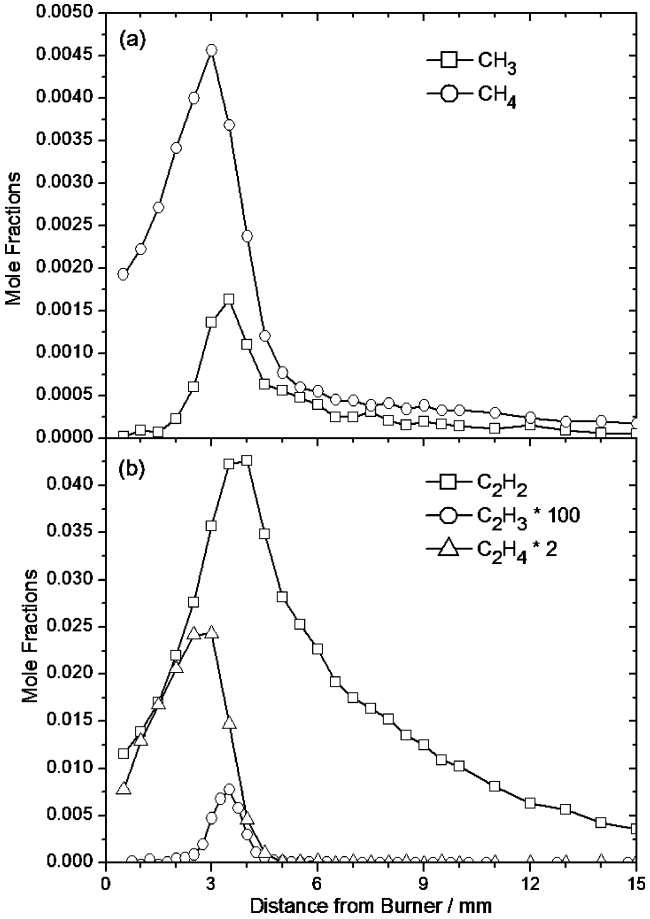

Figure 4. Experimental mole fraction profiles for (a) CH_3 and CH_4 and (b) C_2H_2, C_2H_3, and C_2H_4.

(acetylene), C_2H_3 (vinyl), and C_2H_4 (ethylene). The maximum mole fraction of C_2H_2 is $\sim 4.3 \times 10^{-2}$ at 4.0 mm distance from the burner. The signal from C_2H_3 peaks near $\sim 7.8 \times 10^{-5}$ at 3.5 mm above the burner, while the ethylene mole fraction peaks near $\sim 1.2 \times 10^{-2}$ at 3.0 mm.

The C_2H_2 and C_2H_4 peak mole fractions agree with earlier measurements of Lamprecht et al.[29] to within a factor of 3, while the C_2H_3 concentration differs by a factor of 35. The peak mole fraction of C_2H_3 is lower in the present study. In addition, the C_2H_4 concentration in the earlier study was determined to be larger than the C_2H_2 concentration; however, this is not reproduced here. Good agreement is achieved between the present experimental C_2H_2 and C_2H_4 profiles and the modeled profiles shown in ref 30.

4.4. Mole Fraction Profiles for C_3 Species. Mole fraction profiles for C_3H_2, C_3H_3 (propargyl), C_3H_4 (allene and propyne), and C_3H_5 (allyl) are determined and shown in Figure 5. Propargyl radicals are key intermediates in most flames fueled by aliphatic species, as the propargyl−propargyl self-combination has been found to be the dominant pathway to benzene (or phenyl + H). Modeling indicates that this route also dominates in the fuel-rich cyclopentene flame.[14,30] The propargyl mole fraction peaks at $\sim 3.6 \times 10^{-3}$ near 3.5 mm above the burner. The maximum mole fraction is about a factor of 7 larger than the reported value from Lamprecht et al.[29] but is now in better agreement with previous modeling results.[14,30] Propargyl radicals are primarily formed according to reaction 10 as a decomposition product of cyclopentadienyl radicals and are therefore present in relatively large concentrations:

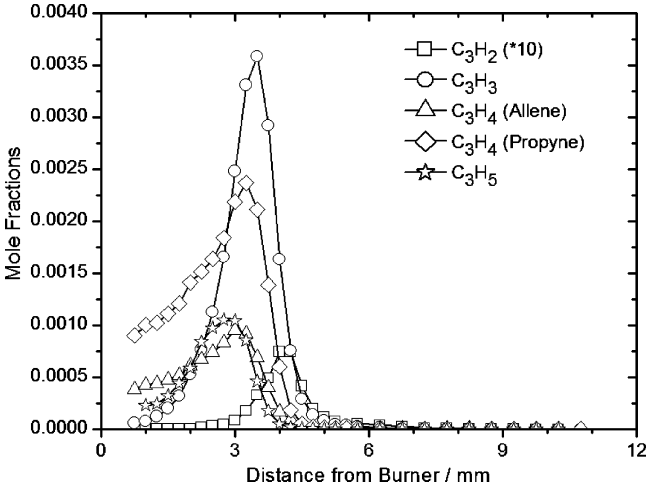

Figure 5. Experimental mole fraction profiles for C_3H_2, C_3H_3, C_3H_4 (allene and propyne), and C_3H_5.

$$\text{cyclo-}C_5H_5 \rightleftarrows \text{linear-}C_5H_5 \rightleftarrows C_2H_2 + C_3H_3 \qquad (10)$$

C_3H_2 is by far the lowest-concentration C_3 species detected with a maximum mole fraction of $\sim 7 \times 10^{-5}$ at 4.0 mm above the burner. C_3H_2 was identified as likely being a mixture of the HCCCH (propargylene) and the cyclo-C_3H_2 (cyclopropenylidene) isomers;[25] however, absolute photoionization cross-sections for both isomers are unknown, and therefore quantitative separation is not undertaken.

The experimental approach allows the determination of mole fraction profiles for the CH_2CCH_2 (allene) and CH_3CCH (propyne) isomers independently. The maximum mole fractions are determined to be 2.4×10^{-3} for propyne and 9.5×10^{-4} for allene. Both profiles peak near 3.25 mm above the burner. The sum of the allene and propyne mole fractions matches the previously reported experimental and modeled value.[14,29]

The mole fraction profile for the allyl radical peaks at 1.0×10^{-3} near 2.75 mm above the burner, in good agreement with earlier experimental results.[29]

4.5. Mole Fraction Profiles for C_4 Species. Mole fraction profiles of C_4H_x ($x = 2-6$, 8) are determined experimentally and summarized in Figure 6. In detail, C_4H_2 is identified by its ionization energy (IE = 10.17 eV)[43] as HCCCCH (diacetylene), and its profile peaks at $\sim 2.9 \times 10^{-3}$ near 4.0 mm, which is close to the earlier experimental and modeled results.[14,29,30] In an earlier work,[26] C_4H_3 and C_4H_5 were identified as mainly CH_2-CCCH (i-C_4H_3) and a mixture of three different C_4H_5 isomers, CH_2CHCCH_2 (i-C_4H_5), CH_3CCCH_2 (methylallenyl), and CH_3-CHCCH. Experimental mole fraction profiles for C_4H_3, and C_4H_5 have been given earlier.[26] However, the analysis procedure has been improved, and the newly derived profiles are included in Figure 6. Maximum mole fractions of $\sim 2 \times 10^{-5}$ (at 3.5 mm) for C_4H_3 and $\sim 4 \times 10^{-5}$ (at 3.0 mm) for C_4H_5 are derived. These numbers are an order of magnitude smaller than the previously published data from Lamprecht et al.[29] Both the electron ionization experiments of Lamprecht et al. and the current work are based on estimated ionization cross-sections; thus, both experimental approaches can possibly lead to large error bars as discussed above. However, the new C_4H_5 maximum mole fraction agrees well with previous and current models.[14]

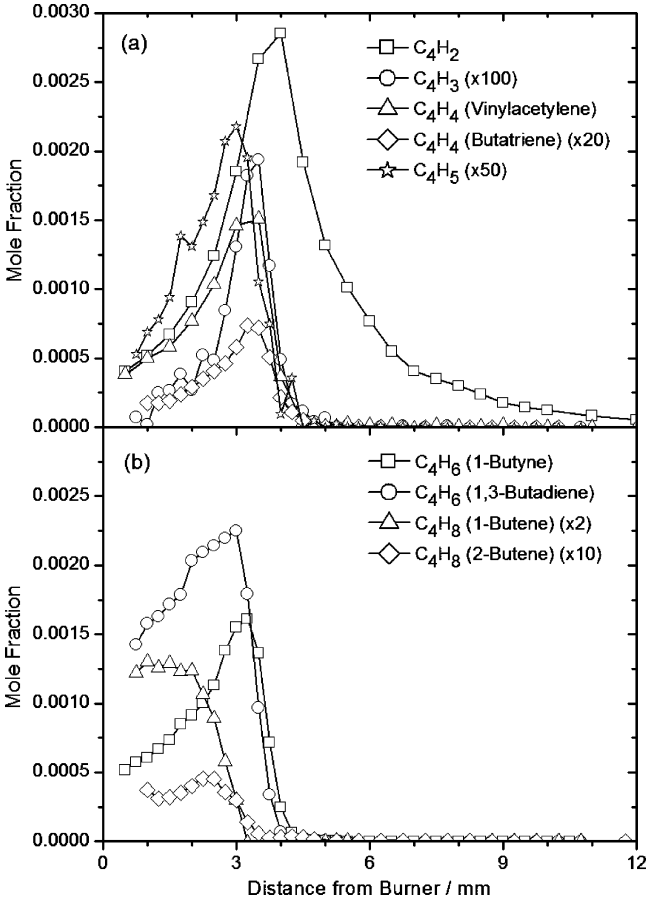

Figure 6. Experimental mole fraction profiles for (a) C_4H_2, C_4H_3, C_4H_4 (vinylacetylene and butatriene), C_4H_5 and (b) C_4H_6 (1,3-butadiene and 1-butyne) and C_4H_8 (1- and 2-butenes).

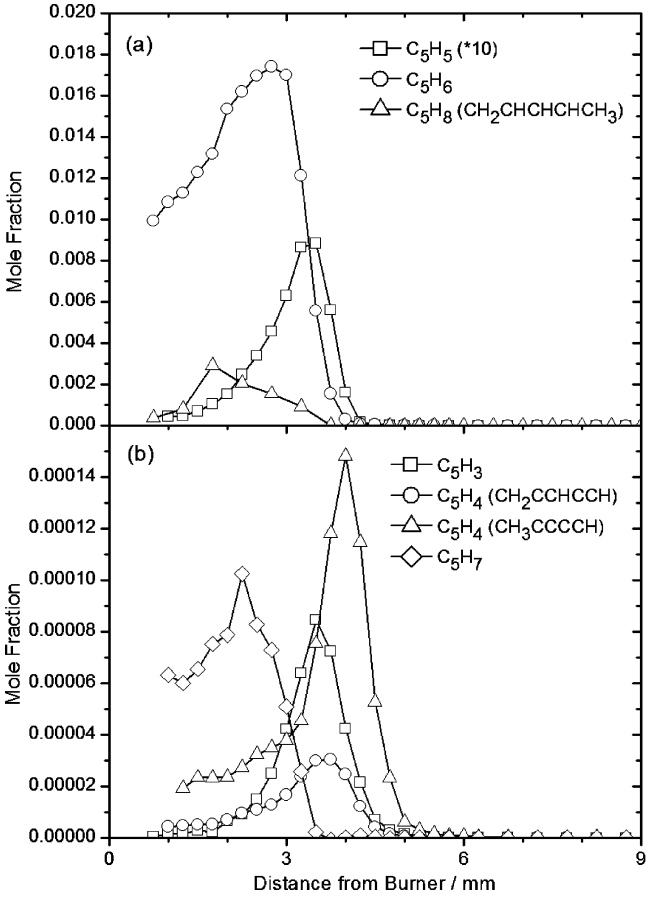

Figure 7. Experimental mole fraction profiles for (a) C_5H_5, C_5H_6, and C_5H_8 (1,3-pentadiene) and (b) C_5H_3, C_5H_4 ($CH_2CCHCCH$ and CH_3-$CCCCH$), and C_5H_7.

The unambiguous identification of $CHCCHCH_2$ (vinylacetylene), CH_2CCCH_2 (butatriene), $CH_2CHCHCH_2$ (1,3-butadiene), $CHCCH_2CH_3$ (1-butyne), $CH_3CHCHCH_3$ (2-butene), and CH_2-$CHCH_2CH_3$ (1-butene) was described in section 3.1. Vinylacetylene and butatriene peak at 3.5 mm above the burner, and the maximum mole fractions are 1.5×10^{-3} and 3.7×10^{-4}, respectively. The sum of the mole fractions of vinylacetylene and butatriene is close to the maximum value reported in the earlier work.[14,29,30] The determined maximum mole fractions for C_4H_6 isomers are 2.3×10^{-3} for 1,3-butadiene and 1.6×10^{-3} for 1-butyne, which is about a factor of 3 larger than previously reported[29] but certainly within the combined error limits of both experiments. C_4H_8 isomers are less abundant than the C_4H_6 isomers in this cyclopentene flame. Maximum mole fractions of 6.5×10^{-4} for 1-butene and $\sim 4 \times 10^{-5}$ for 2-butene are determined. The sum of the C_4H_8 isomer mole fractions is in good agreement with the earlier measurements of Lamprecht et al.[29]

4.6. Mole Fraction Profiles for C_5 Species. Experimentally determined mole fraction profiles of C_5H_x species are shown in Figure 7. Both the *i*- and the *n*-C_5H_3 isomers contribute to the signal at $m/z = 63$.[27] The profile of C_5H_3, which represents the sum of both isomers, peaks at $\sim 8 \times 10^{-5}$ near 3.5 mm above the burner. CH_2CCCCH_2, $CH_2CCHCCH$, and CHC-$CCCH_3$ have been clearly identified at $m/z = 64$.[27] The contribution from CH_2CCCCH_2 is close to the detection limit and therefore neglected. Maximum mole fractions of 1.5×10^{-4} for CH_3CCCCH and $\sim 3 \times 10^{-5}$ for $CH_2CCHCCH$ are determined. The determined C_5H_4 mole fraction is 1 order of magnitude smaller than in previous measurements of Lamprecht et al.,[29] and, in addition to the uncertainty reflected in the combined error of both experiments, it probably indicates the reduced susceptibility of the photoionization measurements to fragmentation problems.

Signal at $m/z = 65$ is dominated by the cyclopentadienyl radical (cyclo-C_5H_5), although minor contributions of at least one linear isomer are detectable.[27] We believe this linear species to be the $CHCCHCHCH_2$ isomer, the second most stable isomer, which is a known isomerization product of cyclopentadienyl.[56,57] The determined mole fraction profile for C_5H_5 peaks at 8.8×10^{-4}. This value is somewhat smaller than that reported in the earlier experiment,[29] but still agrees within the error limits, and is also in good agreement with the model from Lindstedt and Rizos.[14]

The cyclopentadienyl radical is probably the key reactive C_5-ring species in this cyclopentene flame. Cyclo-C_5H_5 is resonantly stabilized and therefore able to build to relatively large concentrations in flames. Its combustion chemistry has been investigated in great detail, including decomposition reactions and reactions converting cyclopentadienyl radicals to aromatic species.[17,20,56−60] As shown in reaction 10, the thermal dissociation and subsequent decomposition of cyclo-C_5H_5 is a major source for propargyl, thus initiating molecular-weight growth.

At $m/z = 66$ (C_5H_6) 1,3-cyclopentadiene is identified by its ionization energy,[61] but the presence of linear isomers, such as $CH_2CHCCCH_3$, $CH_3CHCHCCH$, and CH_2CHCH_2CCH which are detected in other fuel-rich flames,[24,27] cannot be ruled out. However, because of the close link to the fuel species, we believe that the signal at $m/z = 66$ is dominated by 1,3-cyclopentadiene; its experimentally determined maximum mole

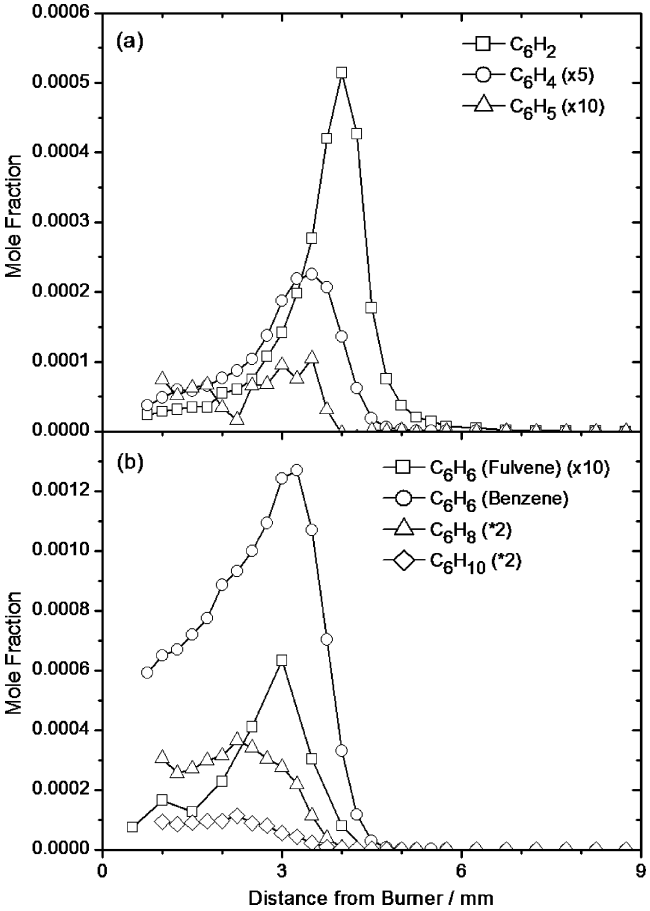

Figure 8. Experimental mole fraction profiles for (a) C_6H_2, C_6H_4, and C_6H_5 and (b) C_6H_6 (benzene and fulvene), C_6H_8, and C_6H_8.

fraction of 1.7×10^{-2} near 2.75 mm above the burner is close to the previously reported value.[29]

The mole fraction profile of C_5H_7 is shown in Figure 7b. Its maximum value is determined to be 1.0×10^{-4} near 2.25 mm above the burner, compared with 2.2×10^{-2} in the earlier measurements.[29] Again, it is conceivable that dissociation of larger molecules, including C_5H_8 (the fuel), into C_5H_7 fragments had resulted in an apparently larger C_5H_7 concentration in the earlier electron ionization measurements.

Cyclopentene (the fuel) and linear isomers contribute to the signal at $m/z = 68$.[27] The signal is overwhelmingly dominated by cyclopentene, which makes it impossible to quantitatively separate mole fraction profiles of linear isomers with ionization energies above that of cyclopentene.[43,62] An ionization threshold of 8.6 eV was observed in the PIE spectrum at $m/z = 68$, suggesting the presence of $CH_2CHCHCHCH_3$ (1,3-pentadiene). The observed flame-sampled photoionization efficiency curve between 8.6 and 9.0 eV matches the cold-flow PIE spectrum of 1,3-pentadiene; thus, other isomers with IEs between 8.6 and 9.0 eV are likely to be absent.[27] The mole fraction profiles of cyclopentene and 1,3-pentadiene are shown in Figures 4 and 7a, respectively. For 1,3-pentadiene a maximum mole fraction of 2.9×10^{-3} near 1.75 mm above the burner is determined.

4.7. Mole Fraction Profiles for C_6 Species. The observed mole fraction profiles for C_6H_x ($x = 2$, 4−6, 8, 10) are shown in Figure 8. The linear 1,3,5-hexatriyne (C_6H_2) and benzyne (C_6H_4) are identified by their ionization energies.[43,63] The 1,3,5-hexatriyne profile shows a sharp peak at 4.0 mm with a maximum mole fraction of 5.1×10^{-4}. The benzyne C_6H_4 signal peaks closer to the burner at 3.5 mm with a maximum mole fraction of $\sim 4 \times 10^{-5}$. The concentration of the phenyl radical (C_6H_5) is just above the detection limit, and the maximum mole fraction of C_6H_5 is determined to be 1×10^{-5} at 3.5 mm above the burner. These values can be compared with the previously published experimental and modeled data.[14,29,30] In this study, the C_6H_2 concentration is determined to be larger by a factor of 2 than in the previous papers but still within the error limits. For C_6H_4 and C_6H_5 the agreement between the experiments is rather poor, and the discrepancies may result from inaccuracies in the estimated absolute photoionization cross-sections and/or fragmentation in the electron ionization experiment. The mole fractions of C_6H_4 and C_6H_5 are a factor of 5 and 10 smaller than in the electron ionization experiments.[29] However, for C_6H_5 the determined maximum mole fraction of 1×10^{-5} is in accord with the modeling predicted value of Kamphus et al.[30]

At least two different C_6H_6 isomers, fulvene and benzene, are unambiguously identified by their ionization energies and/or photoionization efficiency curves.[43,64] These C_6H_6 isomers peak at 3.0 (fulvene) and 3.25 mm (benzene), and the absolute mole fraction for fulvene is determined to be $\sim 6 \times 10^{-5}$, while the mole fraction for the benzene isomer is determined as 1.3×10^{-3}. The C_6H_6 mole fraction profile in this work agrees closely with the one from the previous work, and, furthermore, the maximum mole fraction is comparable to the predicted value.[30]

Benzene (and fulvene) formation are dominated by the propargyl−propargyl self-combination.[14,30] This reaction leads to benzene via linear C_6 species and fulvene (which is easily converted to benzene by H-atom-assisted isomerization):[8,21]

$$C_3H_3 + C_3H_3 \rightleftarrows C_6H_6 \text{ or } (C_6H_5 + H) \qquad (11)$$

Under the fuel-rich conditions in this cyclopentene flame, the reaction sequence (12) is also found to be an important path toward fulvene and benzene:[14]

$$CH_3 + C_5H_5 \rightleftarrows C_5H_4CH_3 + H \rightleftarrows C_5H_4CH_2 \text{ (fulvene)} + H + H \qquad (12)$$

This reaction sequence has been proposed by Moskaleva et al.[20] as a potential source of benzene at high temperatures.

Other pathways leading to benzene or phenyl + H (including *n*-C_4H_3/*n*-C_4H_5 + C_2H_2 and C_5H_3 + CH_3 reactions) have been discussed in the literature;[9,12,21,65−67] however, they have been found to be of little or no importance in this fuel-rich cyclopentene flame.

Cyclohexadiene and cyclohexene are identified at $m/z = 80$ (C_6H_8) and $m/z = 82$ (C_6H_{10}) by their respective ionization energies;[43] their mole fractions peak at 1.7×10^{-4} for C_6H_8 and $\sim 5 \times 10^{-5}$ for C_6H_{10}. The C_6H_8 profile agrees within the error limits with earlier measurements, while the C_6H_{10} has not been quantitatively determined previously.

4.8. Oxygenated Species. Mole fraction profiles for HCO/C_2H_5 (formyl/ethyl), CH_2O (formaldehyde), CH_2CO/C_3H_6 (ketene and propene), CH_3CHO (acetaldehyde), CH_2CHOH (ethenol), and C_6H_5OH (phenol) are presented in Figure 9. All species are identified by their characteristic ionization energies. However, HCO could not be separated from possible contributions from C_2H_5 radicals, and, since the ionization energies, photoionization efficiency curves, and masses of ketene and propene are similar, it is also difficult to separate those species with our current setup. Therefore, propene may contribute to the given ketene profile. According to our experiment, the ketene/propene mole fraction peaks near 4.6×10^{-3}. Lamprecht et al. determined the maxiumum concentration of propene to be 1.1

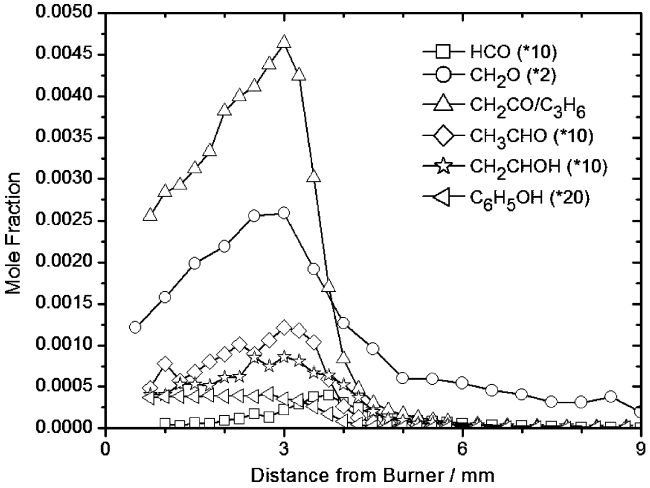

Figure 9. Experimental mole fraction profiles for HCO/C_2H_5, CH_2O, CH_2CO/C_3H_6, CH_3CHO, CH_2CHOH, C_6H_5OH.

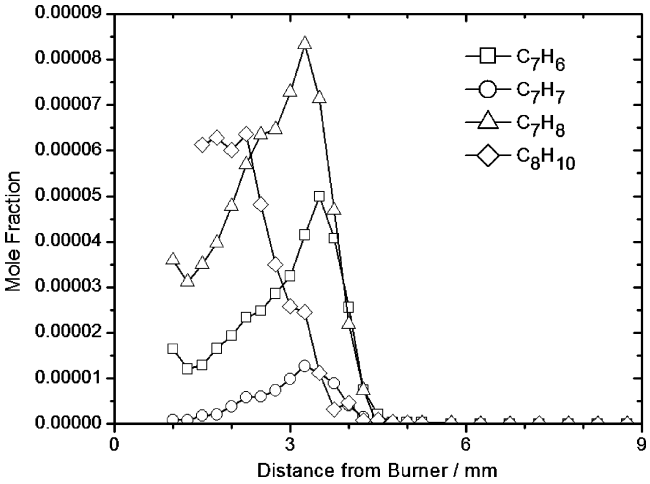

Figure 10. Experimental mole fraction profiles for C_7H_6, C_7H_7, C_7H_8, and C_8H_{10}.

$\times 10^{-3}$, while they did not report the ketene profile.[29] The results, however, suggest that ketene is present in higher concentration than propene. The present study measures the maximum mole fractions of formyl (and/or ethyl) as $\sim 4 \times 10^{-5}$; of CH_2O, 1.3×10^{-3}; of acetaldehyde, 1.2×10^{-4}; of ethenol, $\sim 8 \times 10^{-5}$; and of phenol, $\sim 2 \times 10^{-5}$. The maximum mole fractions for HCO and CH_2O differ significantly from the previous experimental values determined by Lamprecht et al.,[29] who reported 1.2×10^{-4} for HCO and 4.0×10^{-4} for CH_2O.

4.9. C_7 Species and *p*-Xylene. Mole fraction profiles for several C_7 species and *p*-xylene are summarized in Figure 10. Unfortunately, absolute photoionization cross-sections are unknown for all of the presented species; therefore an effective photoionization cross-section of 20 Mb is estimated. We believe that the presented mole fractions are accurate to within a factor of 2−4.

Identification of the C_7H_6 isomer has been discussed in section 3.2. Signal at $m/z = 91$ can be due to the presence of benzyl and/or cycloheptatrienyl radicals. The ionization energies are reported to be 7.24 [68] and 6.236 eV,[69] respectively, and therefore, the available photon energy range is not sufficient to observe ionization thresholds, which are critically needed to identify the isomers. As discussed above, probably cycloheptatriene and toluene contribute to the C_7H_8 signal. The maximum mole fractions are $\sim 5 \times 10^{-5}$ for C_7H_6, $\sim 1 \times 10^{-5}$ for C_7H_7, and $\sim 8 \times 10^{-5}$ for C_7H_8.

We also report the mole fraction profile of *p*-xylene here because one of its likely formation pathways can be considered as an initial step in aromatic ring formation. CH_3CCCH_2 (1-methylallenyl) is a resonantly stabilized methyl-substituted propargyl radical which may react in a manner analogous to the propargyl recombination reaction to form *p*-xylene:

$$CH_3CCCH_2 + CH_3CCCH_2 \rightleftarrows CH_3-C_6H_4-CH_2$$
$$(p\text{-xylyl}) + H \rightleftarrows CH_3-C_6H_4-CH_3 \quad (13)$$

However, at $m/z = 106$ (C_8H_{10}) many different isomers are actually conceivable, including ethylbenzene and *o*-, *m*-, and *p*-xylene. From the observed photoionization efficiency curve, we identify the presence of the *p*-xylene by its ionization energy.[70] We rule out the presence of the ortho- and meta-isomers, but ethylbenzene might contribute to the signal above its ionization energy of 8.77 eV.[71] The maximum mole fraction for C_8H_{10} is determined to be $\sim 6 \times 10^{-5}$.

None of the burner profiles of the C_7 and C_8 species have been reported in earlier experimental and modeling papers.[14,29,30]

5. Conclusions

This paper is part of our continuing effort to analyze the combustion chemistry of cyclopentene in unprecedented detail, employing flame-sampling molecular beam mass spectrometry. The analysis of the flame data is thoroughly discussed, and mole fraction profiles of 49 intermediates are presented with masses ranging from $m/z = 2$ (H_2) to $m/z = 106$ (C_8H_{10}). These data are compared with existing combustion chemistry models, and the results are discussed with regard to the initial steps in fuel consumption and aromatic ring formation. The presented information is critically needed to assist ongoing flame modeling efforts. Mole fraction profiles of several key C_5 species, including C_5H_5, and other known benzene precursors, including, C_3H_3, C_3H_5, C_4H_3, and C_4H_5, are presented. The isomeric compositions are revealed for most species, including allene/propyne and fulvene/benzene. In general, the results are in good agreement with earlier work;[29] nevertheless, some discrepancies for (mainly radical species) are attributed to the use of estimated photoionization cross-sections in the current study and/or fragmentation upon electron ionization in the previous study. The experimental data also compare favorably with the few prior modeling studies.[14,30]

We also describe the isomeric composition of C_4H_x ($x = 4$, 6, 8), C_7H_6, and C_7H_8 species. The isomer resolution is achieved by utilizing easily tunable synchrotron radiation and comparing flame-sampled photoionization efficiency curves with theoretical simulations based on calculated ionization energies and Franck−Condon factors or with cold-flow PIE spectra of the pure substances. With respect to C_4 species, butatriene, vinylacetylene, 1,3-butadiene, 1-butyne, and 1- and 2-butenes are unambiguously identified in this fuel-rich cyclopentene flame. Identification of the $C_5H_4CCH_2/C_5H_5CCH$ isomers and cycloheptatriene and toluene is based on calculated ionization energies, heats of formation, and Franck−Condon factor analyses.

The potential importance of the five-membered C_7H_6 and seven-membered C_7H_8 isomers in molecular-weight growth reactions is discussed. These isomers are of particular interest as they essentially can be formed by reactions of cyclopentadienyl radicals with acetylene. Subsequent reactions of acetylene with radicals generated by H addition or H loss from the C_7H_6 and C_7H_8 rings are potential pathways leading to indene,[31] and thus, the presence of $C_5H_4CCH_2/C_5H_5CCH$ and cycloheptatriene

indicates important pathways toward aromatic species in this fuel-rich cyclopentene flame. These pathways deserve to be explored in future flame chemistry models.

Future work on this cyclopentene flame will be concerned with detailed modeling of the consumption of the fuel, the formation of the aromatic species, and characterization of the growth of aromatic species beyond the first ring, that is, the formation, for example, of indene and naphthalene.

Acknowledgment. The authors are grateful to Paul Fugazzi for expert technical assistance. This work is supported by the Division of Chemical Sciences, Geosciences, and Biosciences, the Office of Basic Energy Sciences, the U.S. Department of Energy, in part under Grants DE-FG02-91ER14192 (P.R.W., M.E.L.) and DE-FG02-01ER15180 (T.A.C., J.W.), and by the Chemical Science Division of the U.S. Army Research Office. The work at Argonne is supported under DOE Contract No. DE-AC02-06CH11357. T.K. and K.K.-H. are supported by the Deutsche Forschungsgemeinschaft under Contract KO 1363/18-3. Sandia is a multiprogram laboratory operated by Sandia Corp., a Lockheed Martin Co., for the National Nuclear Security Administration under Contract DE-AC04-94-AL85000. The Advanced Light Source is supported by the Director, Office of Science, Office of Basic Energy Sciences, Materials Sciences Division, of the U.S. Department of Energy under Contract No. DE-AC02-05CH11231 at Lawrence Berkeley National Laboratory.

Supporting Information Available: Table of photoionization cross-sections and mass discrimination factors. This material is available free of charge via the Internet at http://pubs.acs.org.

References and Notes

(1) Hansen, J.; Sato, M.; Ruedy, R.; Lacis, A.; Oinas, V. *Proc. Natl. Acad. Sci. U.S.A.* **2000**, *97*, 9875.
(2) Jacobson, M. Z. *Nature* **2001**, *409*, 695.
(3) Denissenko, M. F.; Pao, A.; Tang, M. S.; Pfeifer, G. P. *Science* **1996**, *274*, 430.
(4) Durant, J. L.; Busby, W. F.; Lafleur, A. L.; Penman, B. W.; Crespi, C. L. *Mutat. Res.* **1996**, *371*, 123.
(5) Richter, H.; Howard, J. B. *Phys. Chem. Chem. Phys.* **2002**, *4*, 2038.
(6) Frenklach, M. *Phys. Chem. Chem. Phys.* **2002**, *4*, 2028.
(7) Miller, J. A.; Melius, C. F. *Combust. Flame* **1992**, *91*, 21.
(8) Miller, J. A.; Klippenstein, S. J. *J. Phys. Chem. A* **2003**, *107*, 7783.
(9) Westmoreland, P. R.; Dean, A. M.; Howard, J. B.; Longwell, J. P. *J. Phys. Chem.* **1989**, *93*, 8171.
(10) Wang, H.; Frenklach, M. *Combust. Flame* **1997**, *110*, 173.
(11) Atakan, B.; Lamprecht, A.; Kohse-Höinghaus, K. *Combust. Flame* **2003**, *133*, 431.
(12) Walch, S. P. *J. Chem. Phys.* **1995**, *103*, 8544.
(13) McEnally, C. S.; Pfefferle, L. D.; Atakan, B.; Kohse-Höinghaus, K. *Prog. Energy Combust. Sci.* **2006**, *32*, 247.
(14) Lindstedt, R. P.; Rizos, K. A. *Proc. Combust. Inst.* **2002**, *29*, 2291.
(15) Marinov, N. M.; Pitz, W. J.; Westbrook, C. K.; Lutz, A. E.; Vincitore, A. M.; Senkan, S. M. *Proc. Combust. Inst.* **1998**, *27*, 605.
(16) Marinov, N. M.; Pitz, W. J.; Westbrook, C. K.; Vincitore, A. M.; Castaldi, M. J.; Senkan, S. M.; Melius, C. F. *Combust. Flame* **1998**, *114*, 192.
(17) Melius, C. F.; Colvin, M. E.; Marinov, N. M.; Pitz, W. J.; Senkan, S. M. *Proc. Combust. Inst.* **1996**, *26*, 685.
(18) Miller, J. A.; Pilling, M. J.; Troe, J. *Proc. Combust. Inst.* **2005**, *30*, 43.
(19) Westbrook, C. K.; Mizobuchi, Y.; Poinsot, T. J.; Smith, P. J.; Warnatz, E. *Proc. Combust. Inst.* **2005**, *30*, 125.
(20) Moskaleva, L. V.; Mebel, A. M.; Lin, M. C. *Proc. Combust. Inst.* **1996**, *26*, 521.
(21) Pope, C. J.; Miller, J. A. *Proc. Combust. Inst.* **2000**, *28*, 1519.
(22) Cool, T. A.; McIlroy, A.; Qi, F.; Westmoreland, P. R.; Poisson, L.; Peterka, D. S.; Ahmed, M. *Rev. Sci. Instrum.* **2005**, *76*, 094102.
(23) Cool, T. A.; Nakajima, K.; Taatjes, C. A.; McIlroy, A.; Westmoreland, P. R.; Law, M. E.; Morel, A. *Proc. Combust. Inst.* **2005**, *30*, 1681.
(24) Hansen, N.; Miller, J. A.; Taatjes, C. A.; Wang, J.; Cool, T. A.; Law, M. E.; Westmoreland, P. R. *Proc. Combust. Inst.* **2007**, *31*, 1157.
(25) Taatjes, C. A.; Klippenstein, S. J.; Hansen, N.; Miller, J. A.; Cool, T. A.; Wang, J.; Law, M. E.; Westmoreland, P. R. *Phys. Chem. Chem. Phys.* **2005**, *7*, 806.
(26) Hansen, N.; Klippenstein, S. J.; Taatjes, C. A.; Miller, J. A.; Wang, J.; Cool, T. A.; Yang, B.; Yang, R.; Wei, L. X.; Huang, C. Q.; Wang, J.; Qi, F.; Law, M. E.; Westmoreland, P. R. *J. Phys. Chem. A* **2006**, *110*, 3670.
(27) Hansen, N.; Klippenstein, S. J.; Miller, J. A.; Wang, J.; Cool, T. A.; Law, M. E.; Westmoreland, P. R.; Kasper, T.; Kohse-Höinghaus, K. *J. Phys. Chem. A* **2006**, *110*, 4376.
(28) McEnally, C. S.; Pfefferle, L. D. *Combust. Sci. Technol.* **1998**, *131*, 323.
(29) Lamprecht, A.; Atakan, B.; Kohse-Höinghaus, K. *Proc. Combust. Inst.* **2000**, *28*, 1817.
(30) Kamphus, M.; Braun-Unkhoff, M.; Kohse-Höinghaus, K. *Combust. Flame*, submitted for publication.
(31) Fascella, S.; Cavallotti, C.; Rota, R.; Carra, S. *J. Phys. Chem. A* **2005**, *109*, 7546.
(32) Nicholson, A. J. C. *J. Chem. Phys.* **1963**, *39*, 954.
(33) Tanaka, K.; Tanaka, I. *J. Chem. Phys.* **1973**, *59*, 5042.
(34) Cool, T. A.; Nakajima, K.; Mostefaoui, T. A.; Qi, F.; McIlroy, A.; Westmoreland, P. R.; Law, M. E.; Poisson, L.; Peterka, D. S.; Ahmed, M. *J. Chem. Phys.* **2003**, *119*, 8356.
(35) Taatjes, C. A.; Hansen, N.; McIlroy, A.; Miller, J. A.; Senosiain, J. P.; Klippenstein, S. J.; Qi, F.; Sheng, L.; Zhang, Y.; Cool, T. A.; Wang, J.; Westmoreland, P. R.; Law, M. E.; Kasper, T.; Kohse-Höinghaus, K. *Science*, **2005**, *308*, 1887.
(36) Taatjes, C. A.; Hansen, N.; Miller, J. A.; Cool, T. A.; Wang, J.; Westmoreland, P. R.; Law, M. E.; Kasper, T.; Kohse-Höinghaus, K. *J. Phys. Chem. A* **2006**, *110*, 3254.
(37) Becke, A. D. *J. Chem. Phys.* **1993**, *98*, 5648.
(38) Hehre, W. J.; Radom, L.; Pople, J. A.; Schleyer, P. v. R. *Ab Initio Molecular Orbital Theory*; Wiley: New York, 1987.
(39) Frisch, M. J.; Trucks, G. W.; Schlegel, H. B.; Scuseria, G. E.; Robb, M. A.; Cheeseman, J. R.; Montgomery, J. A., Jr.; Vreven, T.; Kudin, K. N.; Burant, J. C.; Millam, J. M.; Iyengar, S. S.; Tomasi, J.; Barone, V.; Mennucci, B.; Cossi, M.; Scalmani, G.; Rega, N.; Petersson, G. A.; Nakatsuji, H.; Hada, M.; Ehara, M.; Toyota, K.; Fukuda, R.; Hasegawa, J.; Ishida, M.; Nakajima, T.; Honda, O.; Kitao, H.; Nakai, H.; Klene, M.; Li, X.; Knox, J. E.; Hratchian, H. P.; Cross, J. B.; Adamo, C.; Jaramillo, J.; Gomperts, R.; Stratmann, R. E.; Yazyev, O.; Austin, A. J.; Cammi, R.; Pomelli, C.; Ochterski, J. W.; Ayala, P. Y.; Morokuma, K.; Voth, G. A.; Salvador, P.; Dannenberg, J. J.; Zakrzewski, V. G.; Dapprich, S.; Daniels, A. D.; Strain, M. C.; Farkas, O.; Malick, D. K.; Rabuck, A. D.; Raghavachari, K.; Foresman, J. B.; Ortiz, J. V.; Cui, Q.; Baboul, A. G.; Clifford, S.; Cioslowski, J.; Stefanov, B. B.; Liu, G.; Liashenko, A.; Piskorz, P.; Komaromi, I.; Martin, R. L.; Fox, D. J.; Keith, T.; Al-Laham, M. A.; Peng, C. Y.; Nanayakkara, A.; Challacombe, M.; Gill, P. M. W.; Johnson, B.; Chen, W.; Wong, M. W.; Gonzalez, C.; Pople, J. A. *Gaussian98*, Revision A11; Gaussian: 2004.
(40) Amos, R. D.; Bernhardsson, A.; Berning, A.; Celani, P.; Cooper, D. L.; Deegan, M. J. O.; Dobbyn, A. J.; Eckert, F.; Hampel, C.; Hetzer, G.; Knowles, P. J.; Korona, T.; Lindh, R.; Lloyd, A. W.; McNicholas, S. J.; Manby, F. R.; Meyer, W.; Mura, M. E.; Nicklass, A.; Palmieri, P.; Pitzer, R.; Rauhut, G.; Schutz, M.; Schumann, U.; Stoll, H.; Stone, A. J.; Tarroni, R.; Thorsteinsson, T.; Werner, H.-J. *MOLPRO*, a package of ab initio programs (designed by H.-J. Werner and P. J. Knowles); 2002.
(41) Cool, T. A.; Wang, J.; Nakajima, K.; Taatjes, C. A.; McIlroy, A. *Int. J. Mass Spectrom.* **2005**, *247*, 18.
(42) Rosenstock, H. M.; McCulloh, K. E.; Lossing, F. P. *Int. J. Mass Spectrom. Ion Phys.* **1977**, *25*, 327.
(43) Bieri, G.; Burger, F.; Heilbronner, E.; Maier, J. P. *Helv. Chim. Acta* **1977**, *60*, 2213.
(44) Parr, A. C.; Elder, F. A. *J. Chem. Phys.* **1968**, *49*, 2659.
(45) Watanabe, K.; Nakayama, T.; Mottl, J. *J. Quant. Spectrosc. Radiat. Transfer* **1962**, *2*, 369.
(46) Kovac, B.; Mohraz, M.; Heilbronner, E.; Boekelheide, V.; Hopf, H. *J. Am. Chem. Soc.* **1980**, *102*, 4314.
(47) Bock, H.; Hirabayashi, T.; Mohmand, S. *Chem. Ber.* **1981**, *114*, 2595.
(48) Ohno, K.; Okamura, K.; Yamakado, H.; Hoshino, S.; Takami, T.; Yamauchi, M. *J. Phys. Chem.* **1995**, *99*, 14247.
(49) Müller, C.; Schweig, A.; Thiel, W.; Grahn, W.; Bergman, R. G.; Vollhardt, K. P. C. *J. Am. Chem. Soc.* **1979**, *101*, 5579.
(50) Taatjes, C. A.; Osborn, D. L.; Cool, T. A.; Nakajima, K. *Chem. Phys. Lett.* **2004**, *394*, 19.
(51) Ramos, C.; Winter, P. R.; Zwier, T. S.; Pratt, S. T. *J. Chem. Phys.* **2002**, *116*, 4011.
(52) Winter, P. R.; Zwier, T. S.; Lehmann, K. K. 55th International Symposium on Molecular Spectroscopy, Columbus, OH, 2000.
(53) Wang, J.; Cool, T. A. To be submitted for publication.
(54) Koizumi, H. *J. Chem. Phys.* **1991**, *95*, 5846.
(55) Trickl, T.; Cromwell, E. F.; Lee, Y. T.; Kung, A. H. *J. Chem. Phys.* **1989**, *91*, 6006.

(56) Burcat, A.; Dvinyaninov, M. *Int. J. Chem. Kinet.* **1997**, *29*, 505.
(57) Moskaleva, L. V.; Lin, M. C. *J. Comput. Chem.* **2000**, *21*, 415.
(58) Roy, K.; Horn, C.; Frank, P.; Slutsky, V. G.; Just, T. *Proc. Combust. Inst.* **1998**, *27*, 329.
(59) Roy, K.; Braun-Unkhoff, M.; Frank, P.; Just, T. *Int. J. Chem. Kinet.* **2001**, *33*, 821.
(60) Burcat, A.; Dvinyaninov, M.; Olchanski, E. *Int. J. Chem. Kinet.* **2001**, *33*, 491.
(61) Derrick, P. J.; Asbrink, L.; Edqvist, O.; Jonsson, B. O.; Lindholm, E. *Int. J. Mass Spectrom. Ion Phys.* **1971**, *6*, 203.
(62) Harris, D.; McKinnon, S.; Boyd, R. K. *Org. Mass Spectrom.* **1979**, *14*, 265.
(63) Zhang, X.; Chen, P. *J. Am. Chem. Soc.* **1992**, *114*, 3147.
(64) Nemeth, G. I.; Selzle, H. L.; Schlag, E. W. *Chem. Phys. Lett.* **1993**, *215*, 151.
(65) Cole, J. A.; Bittner, J. D.; Longwell, J. P.; Howard, J. B. *Combust. Flame* **1984**, *56*, 51.
(66) Frenklach, M.; Clary, D. W.; Gardiner, W. C.; Stein, S. E. *Proc. Combust. Inst.* **1985**, *20*, 887.
(67) Frenklach, M.; Warnatz, J. *Combust. Sci. Technol.* **1987**, *51*, 265.
(68) Im, H. S.; Bernstein, E. R. *J. Chem. Phys.* **1991**, *95*, 6326.
(69) Elder, F. A.; Parr, A. C. *J. Chem. Phys.* **1969**, *50*, 1027.
(70) Bock, H.; Kaim, W.; Rohwer, H. E. *Chem. Ber.* **1978**, *111*, 3573.
(71) Howell, J. O.; Goncalves, J. M.; Amatore, C.; Klasinc, L.; Wightman, R. M.; Kochi, J. K. *J. Am. Chem. Soc.* **1984**, *106*, 3968.
(72) Mamer, O. A.; Lossing, F. P.; Hedaya, E.; Kent, M. E. *Can. J. Chem.* **1970**, *48*, 3606.
(73) Lecoultre, J.; Heilbronner, E.; Muller, P.; Rodriguez, D. *Collect. Czech. Chem. Commun.* **1988**, *53*, 2385.
(74) Brogli, F.; Giovanni, E.; Heilbronner, E.; Schurter, R. *Chem. Ber.* **1973**, *106*, 961.
(75) Lu, K. T.; Eiden, G. C.; Weisshaar, J. C. *J. Phys. Chem.* **1992**, *96*, 9742.
(76) Traeger, J. C.; McLoughlin, R. G. *Int. J. Mass Spectrom. Ion Processes* **1978**, *27*, 319.
(77) Schwell, M.; Dulieu, F.; Gee, C.; Jochims, H. W.; Chotin, J. L.; Baumgärtel, H.; Leach, S. *Chem. Phys.* **2000**, *260*, 261.